**Reference:**

# In-situ TEM stress induced martensitic transformation in Ni$_{50.8}$Ti$_{49.2}$ microwires

Saeid Pourbabak[1], Andrey Orekhov[1], Vahid Samaee[1], Bert Verlinden[2], Jan Van Humbeeck[2], Dominique Schryvers[1]

[1] *EMAT, University of Antwerp, Groenenborgerlaan 171, B–2020 Antwerp, Belgium*

[2] *MTM, Department of Materials Engineering, University of Leuven, Kasteelpark Arenberg 44, 3001 Leuven, Belgium*

In-situ transmission electron microscopy tensile straining is used to study the stress induced martensitic transformation in Ni$_{50.8}$Ti$_{49.2}$. Two microwire samples with different heat treatment are investigated from which one single crystal and three polycrystalline TEM specimens, the latter with micro- and nano-size grains, have been produced. The measured Young's modulus for all TEM specimens is around 70GPa, considerably higher than the averaged 55GPa of the original microwire sample. The height of the superelastic stress plateau shows an inverse relationship with the specimen thickness for the polycrystalline specimens. Martensite starts nucleating within the elastic region of the stress-strain curve and on the edges of the specimens while also grain boundaries act as nucleation sites in the polycrystalline specimens. When a martensite plate reaches a grain boundary in the polycrystalline specimen, it initiates the transformation in the neighboring grain at the other side of the grain boundary. In later stages martensite plates coalesce at higher loads in the stress plateau. In highly strained specimens, residual martensite remains after release.

# 1 Introduction

Near equiatomic Ni-Ti alloys treated with an appropriate heat treatment exhibit shape memory and superelastic properties originating from the underlying martensitic transformation [1], [2]. Although stress induced martensitic (SIM) transformations have been well studied [3]–[7] and utilized [8]–[10] at macroscale, not many quantitative investigations have been performed at the nanoscale, partly due to technical restrictions. Such studies are, however, essential in order to apply Ni-Ti alloys in micromechanical devices and the aim of the present contribution is to show the first results of a series of in-situ experimental investigations of the SIM transformation in nano-sized Ni-Ti material at room temperature and where the microstructural observations are directly coupled to quantitative stress-strain curves. In all cases the starting material is in the austenite phase at room temperature which implies that the observed and induced transformations yield superelasticity at the macro-scale.

Austenitic Ni-Ti alloys under stress can accommodate large strains, mainly due to the SIM transformation [11]. A schematic superelastic stress-strain curve is shown in Figure 1. In such graphs, sometimes three regions are distinguished in the upper part. First, a region of sharp increase of stress versus strain can be recognized between labels a and b in Figure 1 and where elastic deformation of the austenite occurs. Second, a plateau region of stable stress exists between labels b and c in Figure 1 and where the austenite transforms into martensite. With increasing strain martensite plates grow and more can appear, while some of them coalesce into thicker plates. In this plateau region both austenite and martensite phases co-exist and the martensite variant favored by the tensile direction will be dominant [7], [10], [12]–[14]. After the plateau region, between labels c and d in Figure 1, the stress again increases with strain, which is related to the linear elastic deformation of the martensite. When releasing the stress before plastic deformation of the martensite sets in and after a linear martensite elastic relaxation the material returns to its original condition via the lower part of the curve, again showing a constant stress plateau between e and f where now martensite retransforms into austenite, followed by austenite elastic relaxation between f and a [5], [7], [10], [13], [15]. However, dividing such graphs into distinct regions is somewhat misleading since, for example, in between a and b, the slope of the graph can change while at label b the graphs often show a drop in stress before the plateau starts and which is referred to as the "nucleation peak", since the required stress for nucleation of new martensite plates is higher than that for the subsequent propagation and growth of existing plates [6], [16].
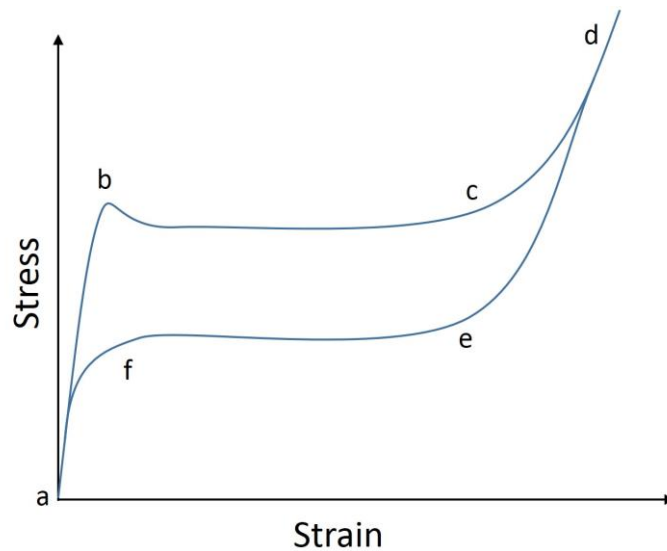
Figure 1 Schematic diagram showing the stress-strain curve of superelastic bulk Ni-Ti.

In-situ straining of thin films [17] or electropolished specimens [18] in a transmission electron microscope (TEM), which allows deformation of a specimen while under observation at the microscale, has been developed in the previous century using conventional in-situ strain holders. This technique has been used by several authors to study microstructural features of SIM transformations in Ni-Ti alloys [19]–[23]. Xu et al. [19] observed that the initial SIM laths nucleate preferentially at grain boundaries, particularly at triple-points, and the strain arising from the end of a lath induces the martensitic transformation in the adjacent grain when the SIM lath grows and reaches a grain boundary. They found the transformation reversible. Jiang et al. [20] reported nucleation and growing martensite upon loading and corresponding shrinkage by unloading, with the reversibility of the movement of the martensite–austenite interface being dependent on the martensite morphology. In the work of Tirry et al. [21], the main conclusion for a polycrystal specimen was the experimental observation of plates of only one variant of martensite and which were reversible upon relaxing. The existence of a compatible interface between austenite and a single variant of martensite was explained in the framework of non-linear elasticity theory [24] by the assumption of slightly deformed austenite and martensite lattices as a result of the imposed strain. Mao et al. [22] performed in-situ tensile tests on micro-strips of different thicknesses prepared by electropolishing combined with focused ion beam (FIB). They found that the transformation occurs first in thicker strips followed by the thinner strips at higher stress and was even completely suppressed in a strip of only 40 nm thick. Pfetzing-Micklich et al. [23] carried out nano-indentation on an austenite Ni-Ti alloy where stress induced martensite is thermally stable at room temperature, followed by post-mortem TEM investigation on the FIB lamella prepared from the indented region. Although this is not strictly speaking an in-situ experiment, they identified martensite plates, as confirmed by B19′ diffraction spots, as needle like features close to the indent. A subsequent in-situ heating of the specimen yielded the reverse transformation to austenite. Although those experiments allow one to observe the transformation during or after straining, they do not provide mechanical data, e.g., stress-strain curves, correlated to the

observed features or mechanisms. The development of novel in-situ TEM straining holders based on micro-electro-mechanical-systems (MEMS) devices and used in the present work allows collecting mechanical data while observing the evolution of the microstructure at the nanoscale and in real time [25], thus providing a more complete and quantitative picture of the behavior of the material under the applied loading conditions.

# 2 Material and methods

A 46.3% cold drawn $Ni_{50.8}Ti_{49.2}$ wire with a diameter of 150μm was annealed at two different conditions, 600°C for 20min and 800°C for 30min, yielding grains up to ~1μm and ~30μm size, respectively. The annealing was followed by room temperature water quenching which prevents precipitation.

A METTLER TOLEDO differential scanning calorimeter (DSC) was used to measure the key parameters of the martensitic transformation and investigate the status of the material at room temperature at which the nano-mechanical tests were performed. A Q800 dynamic mechanical analysis (DMA) machine was used to carry out tensile tests on the microwire and to obtain the macroscopic stress-strain curves.

The wires were embedded in resin after which they were polished using a tripod polisher under an angle of ~10° with respect to the central axis of the wire to obtain a large elliptic cross-section. Dog-bone shaped specimens with lateral sizes of ~ 0.7-1.5×2-3μm were cut from the wires using FIB. The specimen obtained from the large grain size sample (i.e., annealing at 800°C) was cut from a grain interior resulting in a single crystal specimen for the in-situ experiment, while those obtained from the small grain size sample (i.e., annealing at 600°C) contain multiple grains of different sizes. The specimens were then mounted on a Bruker MEMS push-to-pull (PTP) device [25]–[27]. Before the mechanical test, electron energy loss spectroscopy (EELS) was performed on each specimen to measure the thickness [28]. The nano-mechanical tests were performed using a Bruker PI95 PicoIndenter holder in a FEI Osiris instrument running at 200kV. The experiments were carried out in the displacement control mode with a 0.2-0.3nm/s displacement rate yielding a strain rate of about $10^{-4}$/s. The holder provides the quantitative load-displacement data while at the same time a real time movie of the experiment can be obtained under bright field (BF) conditions using the microscope CCD camera; most images shown in this paper are snapshots from these videos. Since the development of the microstructural changes occurs at relatively high speed, i.e., often from one frame to the next, no live diffraction data could be obtained during these running in-situ experiments. Still, some selected area electron diffraction (SAED) data was obtained at the start and finish of particular cycles. The interpretation of the images obtained during the in-situ experiments is thus solely based on the BF contrast, which in some cases is not fully conclusive, in part also since only one tilt axis is available and no tilting can be performed during the in-situ experiment because of risks of instabilities affecting the deformation control. On one occasion the experiment was stopped after the appearance of the first martensite plates (which means that at that moment the displacement was kept constant), in an attempt to obtain diffraction data from an intermediate situation. Unfortunately, the transformation did not stop and the specimen finally fractured so no further data could be gathered this way.

Due to the probable influence of thermal drift on the displacement data obtained from the instrument, the real displacement of the specimens was obtained by image displacement tracking of the deformation movies and accordingly strain amounts were obtained by dividing the raw displacement data by the initial length of the specimen [26]. The load data obtained from the instrument is a combination of the PTP device springs and the force applied on the tensile specimen. Knowing the device spring constant, the force on the specimen can be calculated thus yielding the stress by dividing by the specimen cross-section [25]–[27].

Automated crystal orientation mapping for TEM (Nanomegas® ACOM-TEM [29]) was performed in a FEI Tecnai instrument running at 200kV on one of the polycrystalline specimens to investigate its texture.

One single crystal and three polycrystalline specimens with different thicknesses were investigated. One polycrystalline specimen is chosen perpendicular to the wire direction while the other specimens are taken along the central axis of the wire.

# 3 Results

The austenite finish temperature ($A_f$) of the large and small grain size material was measured by DSC and in all cases found to be below room temperature, which means that the material is in the austenite phase at room temperature, at which all tensile experiments are performed. This is confirmed by TEM observations and selected area electron diffraction (SAED) patterns before each test. Also, no precipitates were found by TEM in any of the specimens, confirming the rapid quench.

## 3.1 Single crystal

Figure 2 (a) represents the in-situ stress-strain curve of the single crystal specimen, having a thickness of 105nm as measured by EELS. The normal to the specimen is close to the $[011]_{B2}$ direction and the pulling direction is close to $[-11-1]_{B2}$ (Figure 2 (a) inset), confirming the $\langle 111 \rangle_{B2}$ texture of a drawn wire [30], [31]. Halfway the region of sharp increase of stress versus strain, at appr. 1.8% strain, the slope of the curve slightly decreases and the remaining stress increase is followed by a stress drop, similar as in the bulk material [6], [32]. The stress plateau, apart from some small fluctuations, remains horizontal up to ~ 12% strain where the specimen fractures. The height of the plateau is ~ 2GPa and the Young's modulus, obtained from the slope of the curve in the austenite elastic deformation between 0 and 0.6% strain (in order to avoid any contribution from the first transforming parts and also used for all following cases), is found to be ~ 77.9GPa.
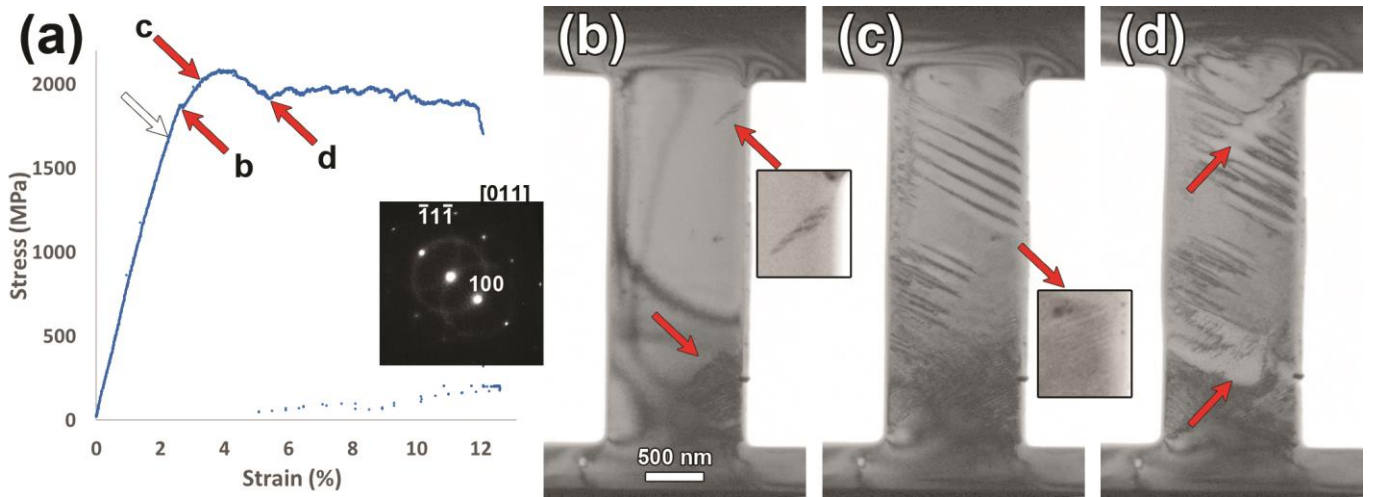
Figure 2 (a) Stress-strain curve of the PTP single crystal specimen, inset: SAED pattern of the specimen revealing a close to $[-11-1]_{B2}$ pulling direction, (b) – (d) different stages of the tensile test obtained as snapshots from the video and corresponding to the points indicated on the stress-strain curve of (a).

Figure 2 (b) – (d) show bright field TEM images of the single crystal specimen at different moments of the tensile test, indicated by solid arrows in Figure 2 (a). From the corresponding TEM video provided as S1 in the supplementary material, the first visible signs of the martensitic transformation occur at ~ 2.2% strain (hollow arrow in Figure 2 (a)) with the appearance of a dark region on the bottom-right side with internal plate-like contrast. A short moment later a single needle appears in the top-right corner in Figure 2 (b), corresponding to point b on the curve, which is at the end of the elastic regime. The latter reveals typical twin variant black/white contrast surrounded by interface contrast separating the plate from the austenite matrix, as seen in the zoom of Figure 2 (b). Upon increasing the strain, more dark parallel plates again clearly resembling martensite microstructure nucleate and grow in different regions of the specimen, as can be seen in Figure 2 (c), some now showing a different variant orientation from those nucleated before as judged from the main direction of the plates and interfaces. Diffraction data obtained from another single crystal specimen strained to about 2.9% and then stopped in an attempt to investigate the nature and microstructure of the transformed region, clearly showed the martensite character of the appearing plates in nearly the entire specimen (as seen from S2 in the supplementary material, also revealing some R phase reflections). Since no in-situ diffraction data could be collected from the specimen in Figure 2, it is unclear whether the major B/W plate-like contrast reveals twinned martensite or single variant plates (dark) with remaining austenite (bright) in between, as seen in earlier qualitative in-situ work [21]. In the latter case, the slight diffraction contrast changes in the bright areas in between the dark plates could be due to small rotations of the austenite lattice. In all cases, the transformation nucleates from one edge of the specimen after which it rapidly propagates to the other side of specimen or the boundary with other martensite variants. In the zoom from the center of the specimen in Figure 2 (c) finer plates can be observed, indicating that already at this early stage martensite appears over the entire length of the gauge. By further pulling the specimen, the contrast of several martensite plates changes and neighboring plates seem to coalesce, from which an intermediate stage is shown in Figure 2 (d). (see also video S1 in supplementary material)

The on-axis stress-strain curve of the original 150μm wire annealed at 800°C for 30 minutes and of which the PTP specimen has been taken is shown as S3 in the supplementary material. In this graph the stress plateau starts at ~ 0.9% strain with a drop in the beginning and ends at ~ 7.3% strain, where the martensite elastic deformation starts. The height of the stress plateau is ~ 380MPa and the Young's modulus is ~ 52.5GPa.

## 3.2 Polycrystalline specimens

Shorter annealing time at lower temperature yields the formation of smaller grains which allows for multiple grains in the PTP specimen. Figure 3 (a) is a BF-TEM image of such a specimen cut along the wire axis and with a thickness of 210nm, revealing grains of 100-500nm size. In order to examine the texture of the specimen ACOM-TEM was performed. The orientation map Figure 3 (b) of this first polycrystalline specimen, further referred to as Poly1, shows the preferential orientation of several grains to be $\langle 111 \rangle_{B2}$ perpendicular to the surface (normal direction ND). The inverse pole figure (IPF) maps in Figure 3 (c) further reveal $\langle 101 \rangle_{B2}$ to be along the pulling direction (PD) of the specimen and with a prominent transverse direction (TD) of $\langle 112 \rangle_{B2}$. Here it should be noted that this particular texture is not necessarily representative for the entire wire, as it was shown by, e.g., Laplanche et al. [30] and Gall et al. [31] that drawn Ni-Ti wires after recrystallization exhibit a strong $\langle 111 \rangle_{B2}$ fiber texture along the wire axis, which apparently is not the case for the region where this particular specimen of $2 \times 0.7 \mu m^2$ was cut.
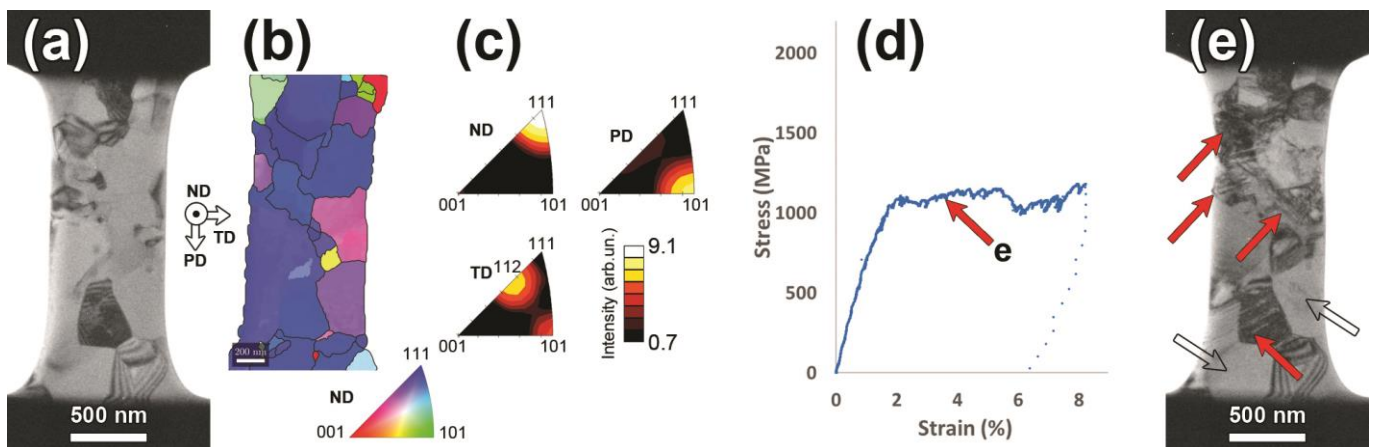


Figure 3 (a) BF-TEM image and (b) ACOM-TEM of the first polycrystalline specimen (Poly1). (c) IPF maps showing strong preferential orientation of $[110]_{B2}$ along the length of the specimen, i.e., the pulling direction (PD), (d) stress-strain curve with an arrow indicating the moment that the image in (e) is taken, (e) BF-TEM image showing transformed and non-transformed grains.

Figure 3 (d) shows the stress-strain curve of the Poly1 specimen. The first transformation occurs at ~ 0.9% and the specimen exhibits elastic deformation of austenite up to ~ 1.8% strain, where the stress plateau starts. Transformation continues to happen in different grains on the stress plateau, however, some grains did not seem to transform even at ~ 8.2% strain where the pulling was stopped (See supplementary material S4 for the TEM video). Figure 3 (e) is taken from the indicated moment on the curve and shows some transformed grains (red solid arrows) while some other grains are still in austenite phase (hollow arrows). The height of the stress plateau is about 1.1GPa and the Young's modulus ~ 76.1GPa.

A second experiment was performed on a specimen with thickness of 220nm, referred to as Poly2 and cut from the same region of the same wire and again along the wire axis. This specimen has a similar $\langle 111 \rangle_{B2}$ ND texture as Poly1, but an average $\langle 211 \rangle_{B2}$ pulling direction (as concluded from the overall SAED pattern in supplementary material S5) and shows the stress-strain curve in Figure 4 (a). The first transformation occurred at 0.6% strain in a 300nm diameter grain, shown in Figure 4 (b), which is clearly not the largest grain in the view. The austenite was elastically deformed up to ~ 1.5% strain where the stress plateau with a small stress drop in the beginning started and continued up to 17.2% deformation, where the pulling was stopped and the specimen was released. At this stage, all but the lower and upper shoulder of the specimen have been transformed into martensite. The height of the plateau is ~ 1GPa and the Young's modulus is ~ 68.5GPa. Figure 4 (c) shows the BF-TEM image of the specimen after release, showing some austenite recovery at the wider top and bottom shoulders of the specimen, seen as a return to a larger area with lower contrast, and with the central part retaining the stronger martensite contrast which confirms the remaining strain of about 13% after unloading. In the S6 video of the Supplementary material it can be seen that nearly halfway the plateau the specimen starts to show necking so that all strain becomes localized in this area finally yielding plastically deformed martensite, explaining the retained martensite after release. The single crystal specimen that was stopped at about 2.9% strain broke at this stage during operation, releasing all strains. SAED showed that also in this case the top and bottom parts of the specimen returned to austenite, while close to the fracture plane, large single variants of martensite remained (as seen from S7 in the supplementary material).
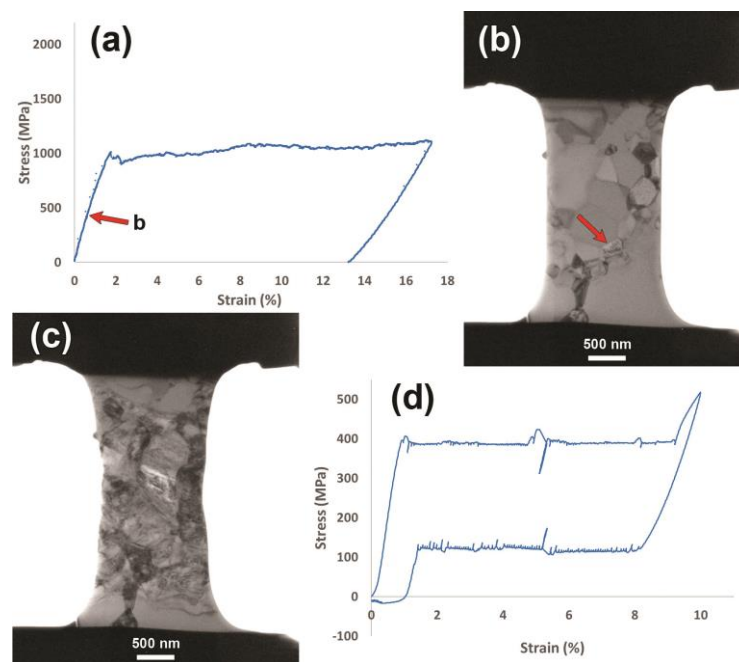


Figure 4 (a) Stress-strain curve of the Poly2 specimen, (b) the first transformation occurring in the indicated grain, (c) the specimen released after the tensile test, (d) stress-strain curve of the entire microwire.

The stress-strain curve of the 150µm wire annealed at 600°C from which both aforementioned nanosized grain PTP specimens were cut is shown in Figure 4 (d). In this graph the plateau starts at ~ 0.9% strain with a small

stress drop in the beginning and ends at ~ 9.2% strain, where martensite elastic deformation starts. The height of the stress plateau is ~ 390MPa and the measured Young's modulus is ~ 57.1GPa.

The stress-strain curve of the third nanosized grain specimen with thickness 160nm, further referred to as Poly3, and cut perpendicular to the axis of the wire annealed at 600°C is shown in Figure 5 (a). The first transformation starts at ~ 0.7% strain. In Figure 5 (b) a BF-TEM image of some fully transformed grains is presented. When a martensite plate reaches the opposite side of the grain, transformation nucleates from the other side of the grain boundary and propagates in the neighboring grain, as shown by arrows in the enlarged image of Figure 5 (c) (see also TEM video supplementary material S8). The plateau of the curve starts at ~ 2.5% strain and continues to ~ 3.7% where the pulling was stopped. After releasing the load, most martensite transformed back to austenite, as seen in Figure 5 (d). The height of the stress plateau is about 1.3GPa and the Young's modulus is ~ 69.6GPa.
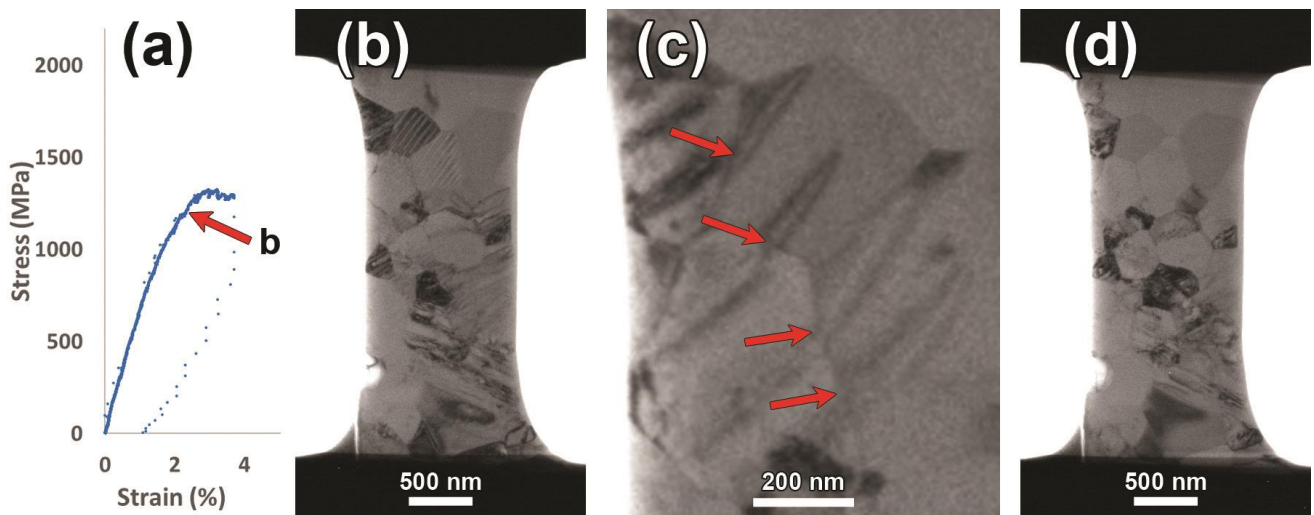


Figure 5 (a) Stress-strain curve of a PTP test on the polycrystalline specimen Poly3 cut perpendicular to the wire axis. (b) BF-TEM image showing several grains transformed into martensite, (c) martensite plates nucleating where an earlier plate in the neighboring grain hits the grain boundary, (d) partial recovery to austenite after releasing the stress.


# 4 Discussion

The results of the different measurements from the four different specimens are combined in Table 1, together with those of the original microwires. At first sight, the stress-strain curves of the four nano-sized specimens resemble the part between labels a and c of the bulk curve shown in Figure 1. They start with a sharp increase of stress during the elastic regime of the austenite. Somewhere along this line, the slope starts to decrease when the first martensite plates appear and in the beginning of the stress plateau a stress drop is observed due to the diminishing of the required stress subsequent propagation and growth of existing plates. This feature is stronger in the single crystal specimen, which could be related to the fact that in this specimen no new plates seem to nucleate after this nucleation peak while for the polycrystalline specimens some grains only transform after the plateau has already started. Depending on the specimen conditions, severe strains can be developed with a

maximum of 17% found in one of the polycrystalline specimens. The nano-mechanical test stress-strain curves do not show the start of elastic transformation of the martensite after the plateau, which possibly corresponds with the fact that in all cases some austenite is still present in the specimen, be it sometimes only at the upper and lower ends where the specimen base becomes wider and the stress decreases.

Table 1 Measures of the examined PTP specimens and the original microwires.

| Single/ poly/ microwire | Thickness | Specimen-wire orientation | Pulling direction (PD) | Surface orientation (ND) | Grain size | Young's modulus (GPa) | Plateau height (GPa) |
|---|---|---|---|---|---|---|---|
| **Large grain microwire** | 150 µm | - | - | - | ~20-30 µm | $52.5 \pm 0.5$ | $0.38 \pm 0.02$ |
| **Single** | $105 \pm 11$ nm | parallel | $\langle 111 \rangle$ | $\langle 011 \rangle$ | - | $77.9 \pm 0.2$ | $1.96 \pm 0.05$ |
| **Small grain microwire** | 150 µm | - | - | - | ~0.1-1 µm | $57.1 \pm 0.3$ | $0.39 \pm 0.01$ |
| **Poly1** | $210 \pm 21$ nm | parallel | $\langle 011 \rangle$ | $\langle 111 \rangle$ | 100-500 nm | $76.1 \pm 0.3$ | $1.08 \pm 0.04$ |
| **Poly2** | $220 \pm 22$ nm | parallel | $\langle 211 \rangle$ | $\langle 111 \rangle$ | 120-950 nm | $68.5 \pm 0.6$ | $1.04 \pm 0.05$ |
| **Poly3** | $160 \pm 16$ nm | normal | - | - | 120-650 nm | $69.6 \pm 0.1$ | $1.29 \pm 0.02$ |

In all of the above examples the Young's modulus for the austenite phase, as determined from the slope of the linear elastic part at the onset of the stress-strain curves, is close to the averaged literature value of ~ 70GPa [33], confirming the accuracy of the quantitative data of the MEMS device. In the case of the single crystal specimen where the pulling direction was along a $\langle 111 \rangle_{B2}$ direction, the measured value is ~ 77.9GPa. All polycrystalline specimens have lower values for the Young's modulus confirming that the $\langle 111 \rangle_{B2}$ direction is a stiff direction [33], [34]. The Young's moduli of the treated microwires are lower than for the single crystal specimen, which can be understood since some grains will not have a $\langle 111 \rangle_{B2}$ stiff direction along the pulling direction. However, the microwire values are also lower than those measured for the polycrystalline PTP specimens, which could be due to the initiation of the stress-induced transformation in the region between labels a and b in Figure 1 where the slope is measured without exactly knowing where the martensite starts [33]. Since the start of the transformation induces a lowering in slope, also the averaged measured Young's modulus will be smaller.

The height of the obtained stress plateaus shows considerable difference for the various samples and specimens investigated. When comparing the 3 in-situ polycrystalline TEM specimens an increase of the stress plateau with decreasing specimen thickness is seen. This confirms the in-situ work by Mao et al. [22] who also found an increase in the needed stress with decreasing specimen thickness to transform small strips of Ni-Ti. They attribute this "size effect" to the increasing influence of non-transforming surface layers with decreasing thickness of the specimen, including a Ga$^+$ impregnated layer caused by FIB and a natural oxide layer, which also enriches Ni in the matrix and thus further suppresses the martensitic transformation. Since also in our case

especially the edges of the specimens are often seen as the nucleation points of the transformation, such surface effects could indeed play an important role. Also the single crystal could fit in this scheme, i.e., it was the thinnest specimen investigated and shows the highest stress plateau, but of course also the overall conditions are very different from the polycrystalline specimens so a quantitative comparison remains difficult. On the other hand, also for thermally induced martensite a decreasing grain size lowers the martensite start temperature [35] so the nanoscale dimensions of the thickness of the specimens should also be considered.

For all specimens, together with elastic deformation of austenite, some martensitic transformation occurs well before reaching the plateau. The transformation accelerates in the beginning of the plateau, where parallel plates of martensite form next to each other, whether it is in the single crystal specimen or in certain grains of a polycrystalline specimen. In the single crystal specimen, many plates very rapidly after nucleation reach the opposite side of the specimen, while in the polycrystalline specimen the grain boundaries form obstacles and some austenite grains need a much higher applied strain to show any sign of transforming to martensite. In many cases, new plates nucleate at sites on grain boundaries where the earlier martensite plates grown in the neighboring grain have ended, confirming the observations of Xu et al. [19]. The plates in the top-left area of the single crystal specimen are further apart than those in the bottom-left and central parts. This can be due to the local width of the austenite area, which is larger on the top since the central and bottom areas are limited by the earlier appearing variant in the bottom-right corner, and the need to balance the elastic strain energy of the austenite/martensite transformation with the surface energy of a single plate [36]–[39]. By increasing the load the martensite plates broaden and seem to merge, which can be associated or with detwinning or reorientation of martensite or with final transformation of any remaining austenite, favoring those variants that best accommodate the external stress and result in single variant parts of the martensite. (in the single crystal specimen this is seen in Figure 2 (d), in the supplementary material S9 an example in the polycrystalline specimen (Figure 3) material is shown) However, without any in-situ SAED support, the exact microstructure of the strong changes in contrast cannot be concluded.

# 5 Conclusions

In-situ TEM tensile tests on nano-scale single crystal and polycrystalline Ni-Ti specimens have been performed. The formation of stress induced martensite is followed and stress-strain curves are plotted based on the mechanical data. The stress plateau height increases by decreasing specimen thickness but remains independent of the grain size since the latter is, on average, larger than the specimen thickness. In all cases the martensitic transformation starts well before the plateau is reached and results in a slight decrease of the slope of the initial sharp increase of the stress-strain curves. When measuring the Young's modulus from the slope before the martensite nucleates, values around 70GPa are found. Martensite transformation starts at edges of the specimen for the single crystal and on the edges and grain boundaries for the polycrystalline specimen. When a martensite plate reaches a grain boundary in the polycrystalline specimen, it initiates the transformation in the neighboring grain at the other side of the grain boundary. After releasing the load some

residual martensite remains in the specimen, the amount depending on the totally induced strain and indicating the existence of induced plasticity in the martensite at large strains.

# 6 Acknowledgements

# 7 Bibliography

[1]    K. Otsuka and X. Ren, "Physical metallurgy of Ti–Ni-based shape memory alloys," *Progress in Materials Science*, vol. 50, no. 5, pp. 511–678, Jul. 2005.

[2]    K. Otsuka and C. M. Wayman, *Shape Memory Materials*. Cambridge University Press, 1999.

[3]    H. Sakamoto, "Distinction between Thermal and Stress-Induced Martensitic Transformations and Inhomogeneity in Internal Stress," *MATERIALS TRANSACTIONS*, vol. 43, no. 9, pp. 2249–2255, 2002.

[4]    S. Miyazaki, K. Otsuka, and Y. Suzuki, "Transformation pseudoelasticity and deformation behavior in a Ti-50.6at%Ni alloy," *Scripta Metallurgica*, vol. 15, no. 3, pp. 287–292, Mar. 1981.

[5]    J. A. Shaw and S. Kyriakides, "Thermomechanical aspects of NiTi," *Journal of the Mechanics and Physics of Solids*, vol. 43, no. 8, pp. 1243–1281, Aug. 1995.

[6]    J. A. Shaw and S. Kyriakides, "On the nucleation and propagation of phase transformation fronts in a NiTi alloy," *Acta Materialia*, vol. 45, no. 2, pp. 683–700, Feb. 1997.

[7]    K. Otsuka, C. M. Wayman, K. Nakai, H. Sakamoto, and K. Shimizu, "Superelasticity effects and stress-induced martensitic transformations in Cu-Al-Ni alloys," *Acta Metallurgica*, vol. 24, no. 3, pp. 207–226, Mar. 1976.

[8]    K. Yamauchi, I. Ohkata, K. Tsuchiya, and S. Miyazaki, Eds., *Shape Memory and Superelastic Alloys*. Woodhead Publishing, 2011.

[9]    T. Yoneyama and S. Miyazaki, *Shape Memory Alloys for Biomedical Applications*. Woodhead Publishing, 2008.

[10]    M. H. Elahinia, *Shape memory alloy actuators: design, fabrication, and experimental evaluation*. Wiley, 2015.

[11]    J. A. Shaw, C. B. Churchill, and M. A. Iadicola, "Tips and Tricks for Characterizing Shape Memory Alloy Wire: Part 1-Differential Scanning Calorimetry and Basic Phenomena," *Experimental Techniques*, vol. 32, no. 5, pp. 55–62, 2008.

[12]    M.-P. Baron and M. Morin, "Stress-Induced Transformation and Temperature-Induced Transformation in Cu-Zn-Al Single Crystals," *J. Phys. IV France*, vol. 07, no. C5, pp. C5-525-C5-530, Nov. 1997.

[13]    A. Rao, A. R. Srinivasa, and J. N. Reddy, *Design of Shape Memory Alloy (SMA) Actuators*. Springer International Publishing, 2015.

[14] T. W. Duerig, *Engineering Aspects of Shape Memory Alloys*. Butterworth-Heinemann, 1990.

[15] D. C. Lagoudas, Ed., *Shape Memory Alloys: Modeling and Engineering Applications*. Springer US, 2008.

[16] L. Truskinovsky and A. Vainchtein, "The origin of nucleation peak in transformational plasticity," *Journal of the Mechanics and Physics of Solids*, vol. 52, no. 6, pp. 1421–1446, Jun. 2004.

[17] H. G. F. Wilsdorf, "Apparatus for the Deformation of Foils in an Electron Microscope," *Review of Scientific Instruments*, vol. 29, no. 4, pp. 323–324, Apr. 1958.

[18] B. Hardiman, W. a. T. Clark, and R. H. Wagoner, "Automated jet polishing of transmission electron microscope specimens for in situ straining," *Journal of Electron Microscopy Technique*, vol. 5, no. 2, pp. 199–202, 1987.

[19] Y. B. Xu, R. J. Wang, and Z. G. Wang, "In-situ investigation of stress-induced martensitic transformation in the Ti-Ni shape memory alloy during deformation," *Materials Letters*, vol. 24, no. 6, pp. 355–358, Sep. 1995.

[20] X. Jiang, M. Hida, Y. Takemoto, A. Sakakibara, H. Yasuda, and H. Mori, "In situ observation of stress-induced martensitic transformation and plastic deformation in TiNi alloy," *Materials Science and Engineering: A*, vol. 238, no. 2, pp. 303–308, Nov. 1997.

[21] W. Tirry and D. Schryvers, "In situ transmission electron microscopy of stress-induced martensite with focus on martensite twinning," *Materials Science and Engineering: A*, vol. 481–482, pp. 420–425, May 2008.

[22] S. C. Mao *et al.*, "Stress-induced martensitic transformation in nanometric NiTi shape memory alloy strips: An in situ TEM study of the thickness/size effect," *Journal of Alloys and Compounds*, vol. 579, pp. 100–111, Dec. 2013.

[23] J. Pfetzing-Micklich, N. Wieczorek, T. Simon, B. Maaß, and G. Eggeler, "Direct microstructural evidence for the stress induced formation of martensite during nanonindentation of NiTi," *Materials Science and Engineering: A*, vol. 591, pp. 33–37, Jan. 2014.

[24] J. M. Ball and R. D. James, "Fine phase mixtures as minimizers of energy," *Arch. Rational Mech. Anal.*, vol. 100, no. 1, pp. 13–52, Mar. 1987.

[25] V. Samaee, R. Gatti, B. Devincre, T. Pardoen, D. Schryvers, and H. Idrissi, "Dislocation driven nanosample plasticity: new insights from quantitative in-situ TEM tensile testing," *Sci Rep*, vol. 8, Aug. 2018.

[26] V. Samaeeaghmiyoni, H. Idrissi, J. Groten, R. Schwaiger, and D. Schryvers, "Quantitative in-situ TEM nanotensile testing of single crystal Ni facilitated by a new sample preparation approach," *Micron*, vol. 94, pp. 66–73, Mar. 2017.

[27] H. Idrissi, C. Bollinger, F. Boioli, D. Schryvers, and P. Cordier, "Low-temperature plasticity of olivine revisited with in situ TEM nanomechanical testing," *Science Advances*, vol. 2, no. 3, p. e1501671, Mar. 2016.

[28] T. Malis, S. C. Cheng, and R. F. Egerton, "EELS log-ratio technique for specimen-thickness measurement in the TEM," *J Electron Microsc Tech*, vol. 8, no. 2, pp. 193–200, Feb. 1988.

[29] E. F. Rauch, J. Portillo, S. Nicolopoulos, D. Bultreys, S. Rouvimov, and P. Moeck, "Automated nanocrystal orientation and phase mapping in the transmission electron microscope on the basis of precession electron diffraction," *Zeitschrift für Kristallographie International journal for structural, physical, and chemical aspects of crystalline materials*, vol. 225, no. 2–3, pp. 103–109, 2010.

[30] G. Laplanche, T. Birk, S. Schneider, J. Frenzel, and G. Eggeler, "Effect of temperature and texture on the reorientation of martensite variants in NiTi shape memory alloys," *Acta Materialia*, vol. 127, pp. 143–152, Apr. 2017.

[31] K. Gall, J. Tyber, V. Brice, C. P. Frick, H. J. Maier, and N. Morgan, "Tensile deformation of NiTi wires," *Journal of Biomedical Materials Research Part A*, vol. 75A, no. 4, pp. 810–823, Dec. 2005.

[32] C. B. Churchill, J. A. Shaw, and M. A. Iadicola, "Tips and Tricks for Characterizing Shape Memory Alloy Wire: Part 3-Localization and Propagation Phenomena," *Experimental Techniques*, vol. 33, no. 5, pp. 70–78, 2009.

[33] P. Šittner, L. Heller, J. Pilch, C. Curfs, T. Alonso, and D. Favier, "Young's Modulus of Austenite and Martensite Phases in Superelastic NiTi Wires," *J. of Materi Eng and Perform*, vol. 23, no. 7, pp. 2303–2314, Jul. 2014.

[34] M. F.-X. Wagner and W. Windl, "Elastic anisotropy of Ni4Ti3 from first principles," *Scripta Materialia*, vol. 60, no. 4, pp. 207–210, Feb. 2009.

[35] T. Waitz, V. Kazykhanov, and H. P. Karnthaler, "Martensitic phase transformations in nanocrystalline NiTi studied by TEM," *Acta Materialia*, vol. 52, no. 1, pp. 137–147, Jan. 2004.

[36] D. Schryvers, "Microtwin sequences in thermoelastic NixAl100-x martensite studied by conventional and high-resolution transmission electron microscopy," *Philosophical Magazine A*, vol. 68, no. 5, pp. 1017–1032, Nov. 1993.

[37] A. L. Roitburd, "Martensitic Transformation as a Typical Phase Transformation in Solids," in *Solid State Physics*, vol. 33, H. Ehrenreich, F. Seitz, and D. Turnbull, Eds. Academic Press, 1978, pp. 317–390.

[38] R. V. Kohn and S. Müller, "Branching of twins near an austenite—twinned-martensite interface," *Philosophical Magazine A*, vol. 66, no. 5, pp. 697–715, Nov. 1992.

[39] A. G. Khachaturyan and G. A. Shatalov, "Theory of Macroscopic Periodicity for a Phase Transition in the Solid State," *Soviet Journal of Experimental and Theoretical Physics*, vol. 29, p. 557, 1969.